47th AIAA/ASME/SAE/ASEE Joint Propulsion Conference & Exhibit
31 July - 03 August 2011, San Diego, California

AIAA 2011-6037

Modeling Interfacial Turbulent Heat Transfer during Ventless Pressurization of a Large Scale Cryogenic Storage Tank in Microgravity

Olga Kartuzova and Mohammad Kassemi

National Center for Space Exploration Research (NCSER)
NASA Glenn Research Center
Cleveland, OH 44135

A two-phase CFD model for pressurization of cryogenic storage tanks is presented using both the Sharp Interface and VOF approaches for representing the phase boundary and the associated interfacial heat, mass and momentum transfer between the liquid and the vapor regions. Both models were validated against the microgravity pressurization data provided by the Saturn S-IVB AS-203 experiment, with the VOF model producing better agreement. Since proper representation of turbulence effects is crucial for predicting interfacial heat and mass transfer with fidelity, two different engineering models for turbulence, namely, the k-ε and the Shear-Stress Transport (SST) k-ω are considered. The fidelity of the two turbulence models for storage tank problems is assessed. The impacts of different turbulent parameters associated with the models, such as initial distributions of the respective turbulent quantities and different interfacial boundary conditions, are also studied. The results of our study underscore the fact that accurate modeling of turbulent interfacial heat transfer is crucial for predicting correct self-pressurization and thermal stratification in the cryogenic storage tank. In this context all the important aspects of turbulent modeling at the interface need to be properly addressed. This includes: 1) initial turbulence level; 2) interfacial turbulence B.C.; 3) the contribution of interface deformations to the enhancement of the interfacial turbulent heat transfer.

Nomenclature

A	=	Area density
E	=	Energy
$\mathbf{g}$	=	Gravity
h	=	Surface curvature
k	=	Turbulence kinetic energy
L	=	Latent heat
M	=	Molar mass of fluid
n	=	Normal vector
p, P	=	Pressure
$\mathbf{q}$	=	Heat flux
Q	=	Heat power
R	=	Gas constant
T	=	Temperature
t	=	time
$\mathbf{v}$	=	velocity

Greek

α	=	Cell value of volume fraction
β	=	Slope limiter
ε	=	Turbulence dissipation rate
ϕ	=	Face value of volume fraction
μ	=	Dynamic viscosity
ρ	=	Density
τ	=	Stress tensor
ω	=	Specific turbulence dissipation rate

Subscripts

i	=	Interface
il	=	Liquid side of the interface
iv	=	Vapor side of the interface
sat	=	Saturation conditions
l	=	Liquid
v	=	Vapor

I. Introduction

Most future space operations depend on the ability to efficiently store, transfer, and manage a variety of single- or multi-phase fluids in the reduced gravity environment.[1] In many situations, especially those pertaining to

future missions to Moon or Mars, cryogens will inevitably play an integral role, both as propellant and life support fluids. Since cryogens are stored at very low temperatures, the storage tanks are quite sensitive to heat leaks from the environment during both on-surface and/or in-Space operations. The heat leaks can originate from a variety of sources including incident solar radiation, planetary albedo, aerodynamic heating, or conduction loads from the tank's support structure. When heat leaks into the tank, it is transported to the liquid–vapor interface by conduction and natural convection causing vaporization. In a closed tank this will result in a pressure rise that must be controlled either by venting or by mixing and cooling the cryogens to safeguard the tanks structural integrity. Accurate assessment of both the pressurization and the associated boil-off rates are, therefore, critically important in defining design requirements for the tank's maximum operating pressure and to project the expected cryogen losses. Since due to prohibitive costs, most of the future cryogenic storage tank designs will be developed without the benefit of in-Space testing, reliance on predictive computational models for storage tank pressurization and pressure control is ever-increasing. But confidence in the models' predictions can only be attained if the models are validated and verified with proper benchmark experimental data.

In 1966, the Saturn IB AS-203 vehicle was launched to provide technology and performance verification of the second (S-IVB) propellant control and engine chill-down systems. This experimental flight also constitutes as the only known sufficiently instrumented, microgravity cryogenic storage tank pressurization test with data that is suited for CFD model validation. In this paper we will present a comprehensive two-phase CFD model for storage tank pressurization that is validated against the AS-203 pressure and temperature data. In modeling the experiment, two different approaches for predicting turbulent heat transfer at the liquid-vapor interface are developed and implemented into the CFD model. In the first approach the interface is modeled using the Volume of Fluid (VOF) method. Here the movement of the interface is diffusely captured while the interfacial energy, mass, and momentum balances are incorporated using source terms in the diffuse interfacial region. In the second approach a sharp stationary interface is considered at the boundary of the two phases where interfacial mass, momentum, and energy balances are rigorously enforced. Through comparison of the predictions generated by these two different interface formulations against each other and against the Saturn S-IVB pressure and temperature data we will underscore the intricate influence of interfacial turbulence on the tank pressurization and the need to capture this effect accurately by the numerical models.

Since the days of the Apollo program, several models with varying levels of sophistication have been developed to both interpret and predict experimental results. Homogeneous thermodynamic analyses are among the earliest models developed to predict the self-pressurization rate in partially filled cryogenic tanks. The homogeneous tank model assumes that the average energy of the liquid and vapor phases changes at the same rate as the energy of the two phase mixture defined at the saturation temperature. Because this assumption of homogeneity is typically not met during the initial phases of self-pressurization experiments, when thermal boundary layers are developing and temperature gradients in the liquid and vapor are not stationary, the agreement between thermodynamics and experiments has generally been poor especially in the initial transient regime.[2-4]

In order to obtain better agreement with experimental data, transport effects must be included. A number of investigators have developed approximate models which account for energy and mass transport. Approximate integral methods,[5] boundary layer related techniques,[6] and zonal methods,[7] for example, have provided better predictions of the tank pressure rise compared to the homogeneous models. However, these models are still severely limited in terms of their general predictive capability. To obtain more meaningful predictions, these approximate techniques have given way to more sophisticated computational models. Lin and Hasan[8] developed a simple conduction model in the liquid and coupled it to the pressurization model of Brown,[9] though rigorous coupling between the phases was lacking. They neglected gas-phase transport but allowed the interface to expand and contract radially. Hochstein et al.[10,11] also neglected the gas-phase transport and employed an effective conductivity model to account for transport in the liquid by performing a cell-by-cell mass balance along the interface to account for evaporation. Their comparisons with experiments[4,12] yielded reasonable agreement for when a tank was heated both uniformly and from the bottom in 1 g. Deviations, however, were noted for the top heating test case in 1 g and for low g uniform heating.

Panzarella and Kassemi[21] rigorously coupled a lumped energy and lumped mass model of the ullage to the transport equations in the liquid, but no experimental comparisons were attempted. A version of this model was also used to study the self-pressurization of large tanks filled with liquid hydrogen in low g[22] and to numerically investigate subcooled jet mixing as a pressure control strategy[23]. Later, Barsi and Kassemi[24] assessed the fidelity of the Panzarella and Kassemi two-phase lumped vapor modeling approach[21] by comparing the model's predictions against ground-based cryogenic self-pressurization data gathered during experiments at the NASA Glenn's K-site facility.[25-27] This model was also expanded to include the effects of heat transfer and fluid flow in the vapor phase

through the solutions of the Navier-Stokes equations and the energy equation in both phases while still lumping the interfacial mass transfer[28].

Grayson et al.[13] also included transport in the ullage and, using the pressurization model of Hirt[14] simulated the AS-203 flight experiment[15,16] with reasonably good agreement. Merte et al.[17] also developed a pressurization model which included the effects of gas-phase transport. The interface was assumed flat and the pressure for the incompressible/incompressible system was updated using a first law energy balance. Merte et al.[18] later compared their predictions with data from the AS-203 flight but the agreement was not good. They attributed the errors to inadequately modeling the tank geometry, and thus the heat distribution along the wall. Val'tsiferov and Polezhaev,[19] included the effects of transport in the ullage and used an integrated form of the ideal gas law to update the pressure but were not able to obtain agreement with Aydelott's self-pressurization experiments.[4] It is apparent from the above mentioned brief review that validation and verification of two-phase storage tank models is not straight forward task rather it has proved to be a formidable and sometimes elusive undertaking.

II. Mathematical Model

A. Governing Equations

A schematic of the Saturn S-IVB storage tank partially filled with liquid hydrogen is shown in Fig. 1. Fluid flow and heat transfer in the tank are described in terms of the continuity, Navier-Stokes and energy equations for both phases:

$$\frac{\partial \rho}{\partial t} + \nabla(\rho \mathbf{v}) = 0 \tag{1}$$

$$\frac{\partial}{\partial t}(\rho \mathbf{v}) + \nabla(\rho \mathbf{v}\mathbf{v}) = -\nabla p + \nabla\left[\mu_{eff}\left(\nabla \mathbf{v} + \nabla v^T\right)\right] + \rho \mathbf{g} + \mathbf{F}_{vol} \tag{2}$$

$$\frac{\partial}{\partial t}(\rho E) + \nabla(\mathbf{v}(\rho E + p)) = \nabla\left(k_{eff} \nabla T\right) + S_h \tag{3}$$

In the present study the liquid phase is treated as incompressible with constant properties, except for the density, which is allowed to vary linearly in the body force term of the momentum equation according to the Boussinesq approximation. The vapor is modeled as compressible ideal gas. All the thermophysical and thermodynamic properties of the fluids are taken from NIST[29] at saturation conditions.

In order to describe liquid-vapor interface, two different approaches are employed. In the first approach the movement of the interface is captured diffusely using the Volume of Fluid (VOF) method, as promogulated by Hirt and Nichols.[30] Here the interfacial energy, momentum and mass balances are applied using source terms in the diffuse interfacial region. In the second approach the interface is assumed to be a sharp rigid boundary between the two phases, where the interfacial balances are rigorously applied. Naturally, this approach is valid for two-phase flow analyses where the interface does not experience significant changes (i.e. when the Bond number is large).

B. VOF Model

In the VOF method a volume fraction is defined in each cell in a way that the volume fractions of all the phases sum to unity. In the cell the change in the interface can be tracked by solving a continuity equation for the volume fraction of the q^{th} phase:

$$\frac{1}{\rho_q}\left[\frac{\partial}{\partial t}\left(\alpha_q \rho_q\right) + \nabla \cdot \left(\alpha_q \rho_q \mathbf{v}_q\right) = S_{\alpha_q}\right], \tag{4}$$

where the volume fraction for the primary phase is determined from:

$$\sum_{q=1}^{n} \alpha_q = 1 \tag{5}$$

In the VOF method the field variables and properties are defined in terms of the volume fraction, which for a general system can be written as:

$$\rho = \sum_{q=1}^{n} \alpha_q \rho_q, \ \mu_{eff} = \sum_{q=1}^{n} \alpha_q \mu_{eff\ q}, \ k_{eff} = \sum_{q=1}^{n} \alpha_q k_{eff\ q} \tag{6}$$

In this fashion, the continuity, momentum and energy equations, as described by Eq. (1) – (3), can be solved throughout the domain for the temperatures and velocities in the two phases. In the VOF model energy (E) and temperature (T) are treated as mass-averaged variables:

$$E = \frac{\sum_{q=1}^{n} \alpha_q \rho_q E_q}{\sum_{q=1}^{n} \alpha_q \rho_q}, \tag{7}$$

where E_q is based on the specific heat of the q^{th} phase and the shared temperature.

Interfacial mass transfer is modeled as a source term in the continuity equation for the volume fraction (Eq. 4), i.e.:

$$S_{\alpha_q} = \dot{\mathbf{m}}_i \cdot \mathbf{A}_i, \tag{8}$$

where $\mathbf{A_i}$ is an interfacial area density vector, $\dot{\mathbf{m}}_\mathbf{i}$ is a mass flux vector, that for near equilibrium conditions can be determined based on the Schrage[32] equation:

$$\left|\dot{\mathbf{m}}\right| = \left(\frac{2\sigma}{2-\sigma}\right)\left(\frac{M}{2\pi R}\right)^{1/2}\left(\frac{P_i}{T_i^{1/2}} - \frac{P_v}{T_v^{1/2}}\right). \tag{9}$$

Here σ is the evaporation efficiency (value of 0.01 was used in this study); M is the molar mass of fluid; R is the universal gas constant; P_i and P_v are, respectively, the interfacial and vapor pressures (it was assumed that $P_i \cong P_{sat}$); T_i and T_v are, respectively, the interfacial and vapor temperatures (it was assumed that $T_i = T_v \cong T_{sat}$ at the interface). Finally, $\mathbf{A_i}$ is defined as:

$$\mathbf{A}_i = \left|\nabla \alpha\right|, \tag{10}$$

where α – volume fraction of the primary phase.

In the present implementation surface tension forces at the interface are modeled via the Continuum Surface Force (CSF) model of Brackbill et al.[33] In this model surface tension forces at the interface are transformed into a volume force ($\mathbf{F}_{vol}$), which is added as a source to the momentum equitation:

$$\mathbf{F}_{vol} = \sum_{\text{pairs}ij,\ i<j} \sigma_{ij} \frac{\alpha_i \rho_i h_j \nabla \alpha_j + \alpha_j \rho_j h_i \nabla \alpha_i}{\frac{1}{2}\left(\rho_i + \rho_j\right)},$$

where h_i is the surface curvature calculated from the local gradients in the surface normal at the interface:

$$h_i = \nabla \cdot \hat{\mathbf{n}} \tag{11}$$

C. Sharp Interface Model

In the Sharp Interface model the governing equations are solved separately for the liquid and vapor domains. The two phases are coupled at the interface through continuity of velocities and shear stresses, as well as, an energy balance performed at the interface boundary:

$$\left|\dot{\mathbf{m}}\right| L = \mathbf{q}_{il} - \mathbf{q}_{iv}. \tag{12}$$

Here $\left|\dot{\mathbf{m}}\right|$ is an interfacial mass transfer rate determined from the previously defined Schrage equation (Eq. 9); $\mathbf{q}_{il}$ and $\mathbf{q}_{iv}$ are conductive heat fluxes on the liquid and vapor sides of the interface:

$$\mathbf{q}_{il} = -k_{l\_eff} \nabla T\,|_l \tag{13}$$

$$\mathbf{q}_{iv} = -k_{v\_eff} \nabla T\,|_v \tag{14}$$

In order to assure velocity continuity at the interface, tangential velocity component from the liquid side of the interface is set equal to the one from the vapor side:

$$v_{\text{tang}\_v} = v_{\text{tang}\_l}, \tag{15}$$

and the tangential component of the interfacial shear stress from the vapor side is applied to the liquid side of the interface:

$$\tau_{\text{tang}\_l} = \tau_{\text{tang}\_v} \tag{16}$$

D. Turbulence modeling

In this study, two different turbulence models were used and compared against each other in the VOF model. The first is the Shear Stress Transport $k\ \omega$ model of Menter[34] (kw-SST), and the second is the Realizable $k\ \varepsilon$

model of Shih et al.[35] (ke-Real). In the cases ran with Sharp Interface model turbulence was modeled using kw-SST model only.

Shear-stress transport $k\ \omega$ model, developed by Menter[34] is similar to the standard $k\ \omega$ model of Wilcox,[36] but has an ability to account for the transport of the principal shear stress in adverse pressure gradient boundary layers. The model is based on the assumption of Bradshaw et al.[37] that the principal shear stress is proportional to the turbulent kinetic energy, which is introduced into the definition of the eddy-viscosity. These features make the kw-SST model more accurate and reliable for a wider class of flows than the standard $k\ \omega$ model.[31]

Realizable $k\ \varepsilon$ model (ke-Real), proposed by Shih et al.,[35] uses an improved dissipation rate equation and "realizable" eddy viscosity formulation. The equation for the model dissipation rate is based on the dynamic equation of the mean-square vorticity fluctuation at large turbulent Reynolds number. In this model eddy viscosity formulation is based on the "realizability" constraints (under certain conditions[35] normal Reynolds stresses may become negative, which is unphysical or unrealizable). For a detailed description of the turbulent models the reader is referred to the Ref. 34 and 35.

In the VOF model continuity of the turbulent quantities is inherently assumed since one set of equations for turbulent kinetic energy and dissipation rate is solved for both phases throughout the domain with properties varying according to the local volume fraction value. Turbulent heat transfer at the interface has an effect on mass transfer and pressure rise in the tank. When Sharp Interface model is applied, there are several ways to model turbulence at the interface: 1) interface could be represented by a wall (turbulent kinetic energy equal to zero, specific dissipation rate near wall is defined according to the turbulence model used); 2) zero gradients for turbulent kinetic energy and specific dissipation rate could be applied at the interface; 3) continuity of turbulent quantities could be applied at the interface (k and ω are calculated from the equality of the gradients on both sides and then values applied to the interface on both sides); 4) correlations could be used in order to define turbulent quantities at the interface. First three approaches are compared in this paper. Fourth approach is needed to be explored; however, it is difficult due to lack of published correlations for interfacial turbulence in microgravity.

III. Numerical Implementation

Both the Sharp Interface model, as well as, the interfacial mass transfer formulation used with the VOF model, have been developed, coded and implemented into a customized in-house version of the Fluent CFD code.

In the Sharp Interface model interfacial energy balance is formulated according to Eq. (12) and incorporated into Fluent via User Defined Function (UDF). The similarly customized UDFs are also used to prescribe interfacial temperature and enforce continuity of tangential velocities and shear stresses across the phase boundary. Because this implementation requires the interface to be represented as a wall, wall B.C. are then naturally used for turbulent quantities. In this case, in addition to enforcing energy balance in the phase change subroutine, appropriate source terms are applied to the vapor mass and energy conservation equations to account for consistent interfacial heat and mass transfer. If instead of turbulent law of the wall, zero gradient and continuity turbulent B.C. are desired for turbulent quantities at the interface, the implementation requires both sides of the interface to be represented as velocity inlets in Fluent. In this case the axial velocity on the vapor side is calculated from the interfacial mass transfer rate. Since liquid compressibility is neglected, zero axial velocity is applied on the liquid side of the interface. In computational cells adjacent to the interface, temperature gradients from Eq. 13 and Eq. 14 are evaluated using the temperatures of the interface and temperatures of the cell centers on the liquid and vapor sides. Interfacial temperature is then calculated based on Eq. 12 in the Newton-Raphson solver with a convergence criterion set to the value of 1.0e-14. All two-phase calculations are performed in the user subroutine, which is called once per outer iteration before any of the field equations are solved.

The computational domain was discretized using unstructured mesh of 24,215 cells as depicted in Fig. 1. In both vapor and liquid domains the conservation equations are evolved in time using second order time stepping routine with the time step size on the order of $1x10^{-2}$ seconds. Second order monotone upwinding scheme is used to discretize the convective fluxes in the momentum, energy and turbulence equations. The PISO method is used for pressure-velocity coupling.

The same discretization techniques are used for the momentum, energy and turbulence equations with the VOF model. Explicit first order scheme is used for time discretization with the VOF model. Lower time step size is required to use with the VOF model compared to the one used with the Sharp Interface model. Time step size used with the VOF model is on the order of 1×10^{-3} seconds. For the volume fraction equation QUICK and Compressive discretization schemes are compared. QUICK-type schemes[39] are based on a weighted average of second-order-upwind and central interpolations of the variable. The compressive scheme is a second order reconstruction scheme

for the VOF equation based on the slope limiter.[31] This scheme became available in ANSYS Fluent R13. In this scheme:

$$\phi_f = \phi_d + \beta \nabla \alpha_d \ , \tag{17}$$

where ϕ_f - face value of *vof*, ϕ_d - donor cell value of *vof*, β - slope limiter, $\nabla \alpha_d$ – donor cell *vof* gradient.

In the VOF model interfacial mass transfer is calculated in the UDF and sources are applied to the momentum and relevant scalar equations based on the assumption that mass "created" or "destroyed" will have the same momentum and energy of the phase from which it was "created" or "destroyed" .[31] Convergence criteria are set to 1 x 10^{-4} for all equations except the energy equation, for which it is set to 1 x 10^{-8}.

IV. Results and Discussion

Case studies presented in this section are based on the 1966 Saturn S-IVB AS-203 closed tank experiment.[38] The tank height is 11.3 m and its radius is 3.3 m. In the present simulations the tank is initially filled with liquid and gaseous hydrogen to a liquid fill level of 32% by volume. Variable tank wall heat fluxes and gravity conditions, applied, are based on the actual flight data.[38] Conduction through the tank wall is not considered and the slosh baffle and deflector walls, located inside the tank, are assumed adiabatic. Initial tank conditions in the present study match experimental ones. Initial tank pressure was set to 12.4 psia (85495 Pa). Uniform temperature of 19.722 K was applied in the liquid and the ullage was assumed to be 2.44 K superheated.

In order to assure grid convergence, three different meshes were considered, as described in table 1. Simulation with the finest grid was only ran for the first 500 seconds because it required significantly longer computational time compared with the medium and coarse grids. All three grids predict similar tank pressures for the first 500 seconds of simulation time, as shown in Fig. 2. Coarse and medium grid predictions are very similar up to 3000 seconds with somewhat lower pressures predicted by the medium grid close to the end of simulation. Medium grid was selected for all consecutive runs in this study.

Table 1. Grid Details.

Grid	# of cells	# of nodes on the interface	y +
Coarse	13,700	100	~ 1
Medium	24,215	350	~ 1
Fine	48,658	700	~ 1

Self-pressurization results generated by two different discretization schemes for the VOF equation are compared in Fig. 3. These schemes are: QUICK and Compressive. As seen in Fig. 3, two discretization schemes, discussed above, result in similar tank pressures. Compressive scheme results in a sharper interface, compared with the QUICK scheme results, therefore it was selected for this study.

As mentioned before, two different turbulence models were considered in this study: the Shear Stress Transport k-omega (kw-SST) of Menter[34] and the Realizable k-epsilon (ke-Real) of Shih et al.[35]. Both turbulence models were tested with the VOF multiphase model and the results are presented in Fig. 4. Both models predict the same values of the tank pressure for the first 2500 seconds of simulation. Later in the run ke-Real predicts lower tank pressures compared with kw-SST model results. In this study kw-SST model was selected for turbulence modeling, since its results match the experimental pressures well.

The effect of initial turbulence level in the tank on the tank pressure rise was studied by applying a high and a low initial turbulence estimations, as summarized in Table 2.

Table 2. Initial Turbulence Details.

Initial Turbulence Guess	*k*, m2/s2	omega, 1/s	distribution
High	0.1	10	uniform
Low	0.01	100	uniform

The results of the runs with different initial turbulence levels in the tank are presented in Fig. 5. Tank pressures predicted in the case of lower initial turbulence match experimental tank pressures. In the case of higher initial turbulence in the tank resulted pressures are lower than experimental ones because of the enhanced heat transfer

from the vapor to the liquid. These results indicate the importance of the initial turbulence conditions in the tank. Ideally, experimental data are required to provide proper initial turbulence conditions for computational study. Lower turbulence guess was used for initial turbulence conditions in the following runs in this study.

Two different approaches to the two-phase flow modeling are compared in this study. Results of the VOF approach are compared with the results of the Sharp Interface method in Fig. 6. In general, tank pressures predicted by the Sharp Interface model are higher than the ones predicted by the VOF model and the experimental ones. Results of three different methods of modeling interfacial turbulence with Sharp Interface model are shown in Fig. 6 for comparison. When Sharp Interface model is utilized, the best comparison with the VOF model and experiment is achieved if the continuity B.C. for turbulent quantities is applied at the interface. This is almost similar to the approach used by the VOF method. Wall interfacial B.C. for turbulence used with the Sharp Interface model, however, predict noticeably higher tank pressures compared with the continuity B.C. and the experimental results. Results from zero gradient turbulent B.C. applied for k and ω at the interface with the Sharp Interface model are the closest to the ones using continuity conditions. Tank pressures predicted using the Flow3D simulation of the Saturn-IVB closed tank experiment by Grayson et al.[13] are also shown in Fig. 6 for comparison. Pressures predicted in the Flow3D VOF simulation are close to the ones from the Fluent VOF results of the present study. However, pressures predicted by the Flow3D VOF deviate more from the experimental ones from 4000 seconds to 5000 seconds, near the end of experiment. In this time frame pressures predicted in the present study with the VOF model match experimental ones quiet well. Also, tank pressure rise curves produced in the present study from all the models do not show seemingly unphysical frequent slope changes that are present in the Flow3D VOF results.

Ullage temperature evolutions from the VOF model and the Sharp Interface model with the continuity and the wall turbulence B.C. at the interface are compared in Fig. 7 with the Flow3D VOF results of Grayson et al.[13] and the experiment. Temperatures predicted by all models match experimental ones up to 3500 seconds of simulation time. Later, VOF and Sharp Interface models predict somewhat lower ullage temperatures compared with the Flow3D VOF and the experiment. There is, however, a degree of uncertainty associated with matching the measurement point location in the ullage used in the experiment. Also, the temperature is measured in close vicinity of the slosh deflector and the top of the tank. The fact that the deflector wall is modeled as adiabatic in the present study could affect temperature distribution in the upper region of the tank. Ideally heat transfer through the slosh deflector wall should be considered.

Liquid temperature evolutions from our three different computational models and the Flow3D VOF model are compared with experimental ones in Fig. 8. The present Fluent VOF model matches the experiment closely. The Flow3D VOF model predicts significant large amplitude oscillation in the liquid temperature at the measurement location with the values drastically above and below experimental ones, which, again, seems to be unphysical. The Sharp Interface model with both wall and continuity interfacial turbulence B.C. predicts lower temperatures than the experimental ones. These differences all point to the importance of the interfacial turbulence on the liquid temperature.

The temperature contours in the tank at the end of simulation are presented in Fig. 9. Results of the Sharp Interface model with continuity B.C. for the interfacial turbulence are compared with the Fluent VOF and the Flow3D VOF predictions. All models predict high temperature regions located underneath the slosh deflectors and the high temperature vortexes shedding by the deflectors. Temperature distributions in the tank, however, differ among the models. Sharp Interface model predicts less variation in tank temperatures compared with both VOF models. It predicts higher temperature region near the top of the tank and lower temperatures at the interface. However, temperatures near the interface predicted by the Sharp Interface model are higher than the ones predicted by the Fluent and the Flow3D VOF models. Fluent VOF model predicts slightly higher temperatures at the top of the tank compared with the Sharp Interface model, but lower than the ones predicted by the Flow3D VOF model. Similar temperatures are predicted near the interface by two VOF models. It is interesting to note that while a nearly flat interface is predicted by the Fluent VOF model near the end of simulation, as shown in Fig. 9, Flow3D VOF predicts noticeable deformation of the interface near walls and at the center of the tank.

The velocity fields at 5380 seconds, as predicted by the Sharp Interface, Fluent VOF and Flow3D VOF models are presented in Fig. 10. The Sharp Interface and the Fluent VOF models predict high velocity recirculation region between the slosh deflector and the top of the tank. Fluent VOF predicts somewhat higher velocities near the interface, especially on the liquid side. This is due to the interface movement that is absent in the Sharp Interface model. Tank velocity field predicted by the Flow3D VOF model differs from the ones predicted by the Fluent VOF and the Sharp Interface models. The Flow3D VOF model predicts a high velocity region at the center of the tank below the slosh deflector. These high velocities may be caused by interfacial deformations near the tank axis.

Interfacial mass transfer rate evolutions predicted by the present Fluent VOF model and the Sharp Interface model with the continuity and the wall turbulent B.C. are compared in Fig. 11. All models predict initial

condensation (negative values). The VOF model predicts condensation during the entire simulation with an average value of 0.005 kg/s. The Sharp Interface model with the wall B.C. for interfacial turbulence predicts evaporation between 200 seconds and 1200 seconds and condensation with an average value of 0.001 kg/s for the remaining time. The Sharp Interface model with the continuity turbulent B.C. predicts evaporation for the most of the simulation time with almost zero net interfacial mass flow rate between 2000 and 3500 seconds. It is interesting to note that despite these large differences in the interfacial mass flow rates predicted by the models, their effect on the tank pressure rise is very small. Thus most of the contribution to pressure rise in the vapor is due to interfacial and non-wetted wall heat transfer.

Interfacial heat power evolutions obtained from the Sharp Interface models with the continuity and the wall B.C. for the interfacial turbulence are compared in Fig. 12. Heat input into the tank is, also, plotted on this figure for comparison. Negative values of the interfacial heat power, predicted by both models, indicate that heat is going from the vapor into the liquid region. The Sharp Interface model with the continuity B.C. for interfacial turbulence predicts average interfacial heat power added from the vapor to the liquid on the order of 10000 W. Difference between Q_{il} and Q_{iv}, which represents interfacial mass transfer rate, is very small. The same model with the wall B.C. for turbulent quantities at the interface predicts much less heat coming from the vapor into the liquid region compared to the continuity B.C. case. This means that in this model more heat remains in the vapor region and is responsible for the higher tank pressures compared with the continuity B.C. case. Heat input into the tank varies in time in experiment and has an average value of 30000 W. Comparing this value with an average interfacial heat power from the Sharp Interface model with continuity B.C. one can see that only about one third of the heat entering the tank is transported to the interface; the rest of the heat goes into the raising the tank temperature and pressure.

One of the reasons responsible for the difference between tank pressures predicted by the VOF and the Sharp Interface models is an increase in interfacial area in the VOF model due to the interface deformation. The initial vapor-liquid interface deformation, predicted by the VOF model, is compared in Fig. 13 to the deformation at the middle (t = 3243 s) and the end (t = 5380 s) of the experiment. At the beginning of simulation interface is flat with an area of 34.21 m^2. Interfacial area increases to the value of 34.25 m^2 by 3243 seconds with noticeable interface deformation at this time. Further interface deformation and interfacial area increase happens at the end of simulation at 5380 seconds where the interfacial area is increased to 34.30 m^2. This observation suggests that even if interfacial heat fluxes are equal in the Sharp Interface and the VOF models, the VOF model will account for larger amount of heat going from the vapor into the liquid due to the increased interfacial area. Therefore, tank pressures predicted by the VOF model are lower compared to the ones predicted by the Sharp Interface model. Another explanation for the difference in tank pressures predicted by the VOF and Sharp Interface models is that movement of the interface in the VOF model raises turbulence and, therefore, enhances heat transfer at the interface. Sharp Interface with law of the wall model predicts lower interfacial turbulence and under-predicts heating of the liquid by the vapor, which results in higher vapor pressure compared to the experiment. To illustrate this point turbulence kinetic energies on both liquid and vapor sides of the interface are plotted in Fig. 14 at t = 5380 s. Here the origin is taken at the tank axis and 3.3 m is at the tank wall. It is apparent that the VOF model predicts higher turbulence on both sides of the interface compared with the Sharp Interface model. Turbulence level on the liquid side of the interface predicted by the VOF model is just slightly lower than on the vapor side. Sharp Interface model with continuity interfacial turbulence B.C. predicts less turbulence at the interface compared with the VOF model, but much higher turbulence compared with the Sharp Interface model with the wall interfacial turbulent B.C. Thus, significantly lower turbulence on the vapor side than on the liquid side is predicted by the Sharp Interface model, while the VOF model predicts almost equal turbulence on both sides of the interface. This suggests that movement of the interface significantly increases amount of turbulence, especially on the vapor side of the interface, and enhances interfacial heat transfer, thus pulling more heat from the vapor into the liquid region and reducing the tank pressure. In case of the Sharp Interface model with the wall B.C. turbulence kinetic energy approaches zero value at the interface and effective thermal conductivities of the liquid and vapor hydrogen are equal to the molecular ones (see Fig. 15). When continuity B.C. is applied for turbulent quantities at the interface (in both the VOF and the Sharp Interface models) effective thermal conductivities at the interface increase drastically for both phases compared to the molecular values.

V. Conclusion

A two-phase CFD model for pressurization of cryogenic storage tanks was presented using both the Sharp Interface and the VOF approaches for representing the phase boundary and the associated interfacial heat, mass and momentum transfer between the liquid and the vapor regions. Both models were validated against the microgravity pressurization data provided by the Saturn S-IVB AS-203 experiment with the VOF model producing better

agreement. The results of our study underscore the fact that accurate modeling of turbulent interfacial heat transfer is crucial for predicting correct self-pressurization and thermal stratification in the cryogenic storage tank. In this context all the important aspects of turbulent modeling at the interface need to be properly addressed. This includes: 1) initial turbulence level; 2) interfacial turbulence B.C.; 3) the contribution of interface deformations to the enhancement of the interfacial turbulent heat transfer.

It seems that with proper implementation the VOF model has the capability of representing all the three above mentioned components with adequate fidelity. However, the VOF model requires quite small time steps in order to capture the interface movement accurately. This results in substantial computational resources and long computational times. On the other hand, the Sharp Interface model can simulate the storage tank pressurization with much more reasonable resources and faster run times. However, while the Sharp Interface model with the continuity interfacial B.C. may accurately model the first two turbulent components, it cannot readily account for the important effect of the interfacial deformation on turbulent heat transfer.

Acknowledgments

This work was supported by NASA's Exploration Technology Development Program Office under the Cryogenic Propellant Storage and Transfer Project. Valuable insight provided through numerous discussions with Dr. Jeff Moder of the Combustion Branch at NASA Glenn Research Center, are gratefully acknowledged.

References

[1]Salzman, J., "Fluid management in space-based systems," *Proceedings of the Engineering, Construction, and Operations in Space, 5th international conference on space*, Vol. 1, 1996, p. 521–6.

[2]Knoll, R., Smolak, G., Nunamaker, R., "Weightlessness experiments with liquid hydrogen in aerobee sounding rockets; uniform radiant heat addition – flight 1," NASA TM X-484, 1962.

[3]Aydelott, J., Corpus, E., Gruber, R., "Comparison of pressure rise in a hydrogen dewar for homogeneous, normal-gravity, quiescent, and zero gravity conditions – flight 9," NASA TM X-1052, 1965.

[4]Aydelott, J., "Normal gravity self-pressurization of 9-inch (23 cm) diameter spherical liquid hydrogen tankage," NASA TN D-4171, 1967.

[5]Bailey, T., Vandekoppel, R., Skartvedt, G., Jefferson, T., "Cryogenic propellant stratification analysis and test data correlation," *AIAA Journal*, 1963, 1:1657–9.

[6]Arnett, R., Voth, R., "A computer program for the calculation of thermal stratification and self-pressurization in a liquid hydrogen tank," NASA CR 2026, 1972.

[7]Nguyen, H., "Zero-g thermodynamic venting system (TVS) performance prediction program," Tech Rep, Rockwell Aerospace, 1994.

[8]Lin, C., Hasan, M., "Self-pressurization of a spherical liquid hydrogen storage tank in a microgravity environment," NASA TM 105372, 1992.

[9]Brown, J., "Vapor condensation on turbulent liquid," Ph.D. dissertation, MIT, Cambridge, MA, 1991.

[10]Hochstein, J., Ji H-C, Aydelott, J., "Effect of subcooling on the on-orbit pressurization rate of cryogenic propellant tankage," AIAA 86–1253, 1986.

[11]Hochstein, J., Ji H-C, Aydelott, J., "Prediction of self-pressurization rate of cryogenic propellant tankage," *J. Propulsion and Power*, 1990, Vol. 6, No.1, 11–7.

[12]Abdalla, K., Frysinger, T., Androcchio, C., "Pressure-rise characteristics for a liquid hydrogen dewar for homogeneous, normal gravity, quiescent, and zero-gravity tests," NASA TM X-1134, 1965.

[13]Grayson, G.D., Lopez, A., Chandler, F.O., Hastings L.J., Tucker, S.P., "Cryogenic Tank Modeling for the Saturn AS-203 Experiment," *Proceedings of the 42nd AIAA/ASME/SAE/ASEE Joint Propulsion Conference*, AIAA 2006-5258, 2006.

[14]Hirt, C., "Modeling phase change and homogeneous bubbles," FSI-01-TN57. Flow Science Inc., 2001.

[15]Bradshaw, R., "Evaluation and application of data from low gravity orbital experiment phase I – final report," NASA CR-109847, 1970.

[16]Navickas, J., Madsen, R., "Propellant behavior during venting in an orbiting Saturn S-IVB stage", *Advances in cryogenic engineering*, Vol. 13, Plenum Press; 1968. p. 188–98.

[17]Merte, H., Clark, J., Barakat, H., "Finite difference solution of stratification and pressure rise in containers", Tech rep, Heat Transfer Laboratory, University of Michigan, Tech Report No. 4, 1968.

[18]Merte, H., et al., "Transient pressure rise of a liquid–vapor system in a closed container under variable gravity", *Proceedings of the 4th International Heat Transfer Conference*, Paris, France, 1970.

[19]Val'tsiferov, Y., Polezhaev, V., "Convective heat transfer in a closed axisymmetric vessel with curvilinear generatrix in the presence of phase boundaries and phase transitions," *Izv Akad Nauk SSSR, Mekh Zhidk Gaza*, 1975, 6:126–34.

[20]Amirkhanyan, N., Cherkasov, S., "Theoretical analysis and procedure for the calculation of thermophysical processes occurring in a cryogenic vessel under conditions of non-vented storage," *High Temp.*, 2001, Vol. 39, No. 6, 905–11.

[21]Panzarella, C., Kassemi, M., "On the validity of purely thermodynamic descriptions of two-phase cryogenic fluid storage," *J Fluid Mech*, 2003, 484:41–68.

[22]Panzarella, C., Kassemi, M., "Self-pressurization of large spherical cryogenic tanks in space," *J. Spacecraft Rocket*, 2005, 42:299–308.
[23]Panzarella, C., Plachta, D., Kassemi M., "Pressure control of large cryogenic tanks in microgravity," *Cryogenics*, 2004, 44:475–83.
[24]Barsi, S., Kassemi, M., "Numerical and Experimental Comparisons of the Self-Pressurization Behavior of an LH2 Tank in Normal Gravity," *Cryogenics*, Vol. 48(3/4), 2007, pp. 122-129.
[25]Stochl, R., Knoll, R., "Thermal performance of a liquid hydrogen tank multilayer insulation system at warm boundary temperatures of 630, 530, and 152 R," NASA TM-104476, 1991.
[26]Dresar, N. V., Lin, C., Hasan, M., "Self-pressurization of a flightweight liquid hydrogen tank: effects of fill level at low wall heat flux," NASA TM-105411, 1992.
[27]Hasan, M., Lin, C., Dresar, N., V., "Self-pressurization of a flightweight liquid hydrogen storage tank subjected to low heat flux," NASA TM-103804, 1991.
[28]Barsi, S., Panzarella, C. H., Kassemi, M., "An Active Vapor Approach to Modeling Pressurization in Cryogenic Tanks," *Proceedings of the 43rd AIAA/ASME/SAE/ASEE Joint Propulsion Conference*, AIAA 2007-5553, Cincinnati, OH, 2007.
[29]Lemmon, E.W., McLinden, M.O., and Friend, D.G., "*Thermophysical Properties of Fluid Systems*" in NIST Chemistry WebBook, NIST Standard Reference Database Number 69, Eds. Linstrom, P.J., and Mallard, W.G., National Institute of Standards and Technology, Gaithersburg MD, 20899, http://webbook.nist.gov.
[30]Hirt, C.W., and Nichols B.D., "Volume of fluid (VOF) method for the dynamics of free boundaries," *Journal of Computational Physics*, Vol. 39 No. 1, 1981, pp. 201-225.
[31]ANSYS Fluent Documentation. Release 13.0. November 2010.
[32]Schrage, R.W., A *theoretical study of interphase mass transfer*, Columbia University Press, New York, 1953.
[33]Brackbill J.U., Kothe, D.B., Zemach, C., "A continuum method for modeling surface tension," *J. Comp. Phys.* Vol. 100, 1992, pp. 335–354.
[34]Menter, F. R., "Two-Equation Eddy-Viscosity Turbulence Models for Engineering Applications," *AIAA Journal*, Vol. 32 No. 8, 1994, pp. 1598-1605
[35]Shih, T.H., Liou, W.W., Shabbir, A., Yang, Z., Zhu, J., "A New *k-ε* Eddy Viscosity Model for High Reynolds Number Turbulent Flows," *Computers Fluids*, Vol. 24, 1994, pp. 227-238.
[36]Wilcox, D.C., *Turbulent Modeling for CFD*, DCW Industries, Inc., La Canada, California, 1998
[37]Bradshaw, P., Ferriss, D.H., and Atwell, N.P., "Calculation of Boundary-Layer Development Using the Turbulent Energy Equation," *Journal of Fluid Mechanics*, Vol. 28, No. 3, 1967, pp. 593-616.
[38]Ward, W.D., et al., "Evaluation of AS-203 Low-Gravity Orbital Experiment," NASA CR 94045 (Chrysler Corp. Space Div. Technical Report BB-3.4.3-5-101), 13 January 1967.
[39]Leonard, B. P., and Mokhtari, S., "ULTRA_SHARP Nonoscillatory Convection Schemes for High-Speed Steady Multidimentional Flow," NASATM1-2568 (ICOMP-90-12), 1990.

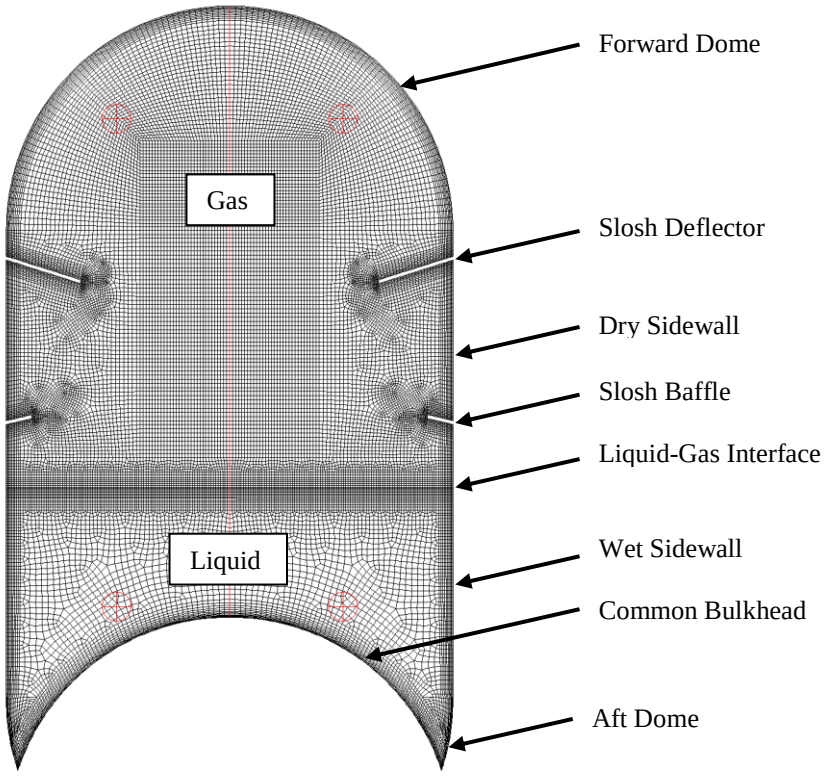

Figure 1. Computational domain with grid details and locations of the temperature measurement points in the liquid and vapor regions.

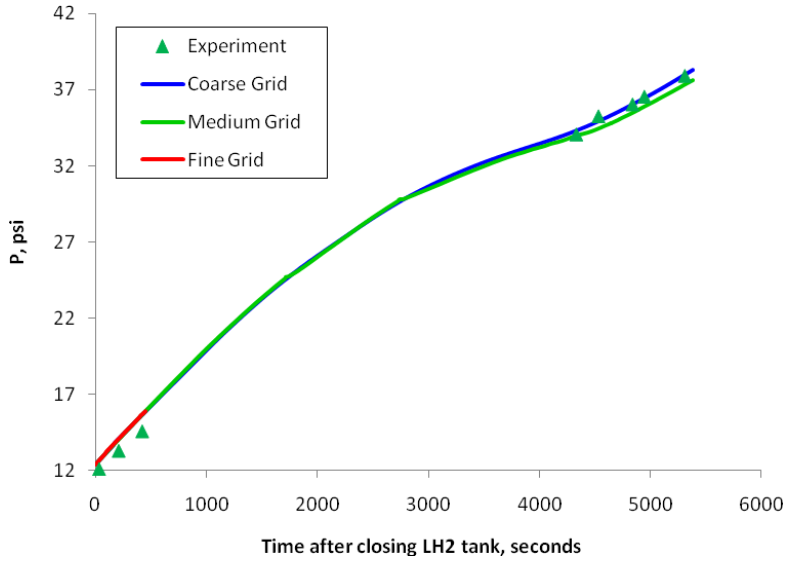

Figure 2. Pressure evolution in the Saturn-IVB tank during closed tank stage (Grid Independence Study with VOF multiphase model)

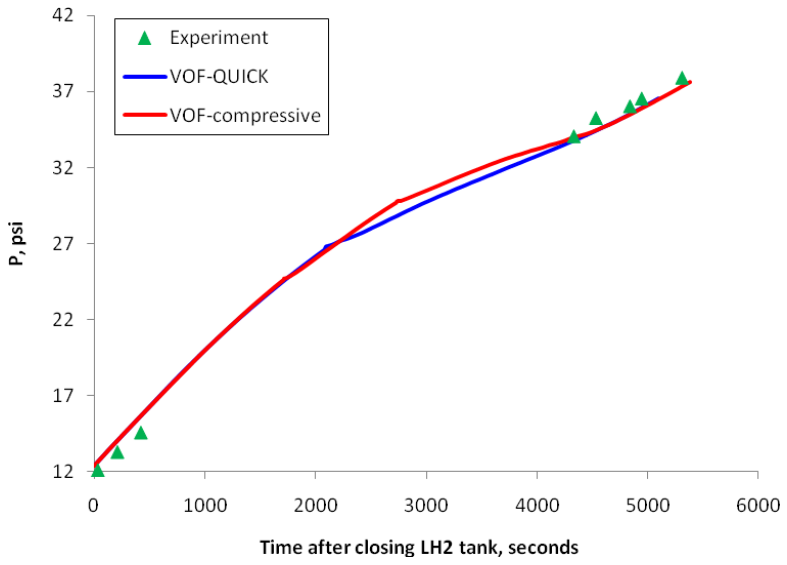

Figure 3. Pressure evolution in the Saturn-IVB tank during closed tank stage (QUICK versus Compressive discretization scheme for the VOF equation)

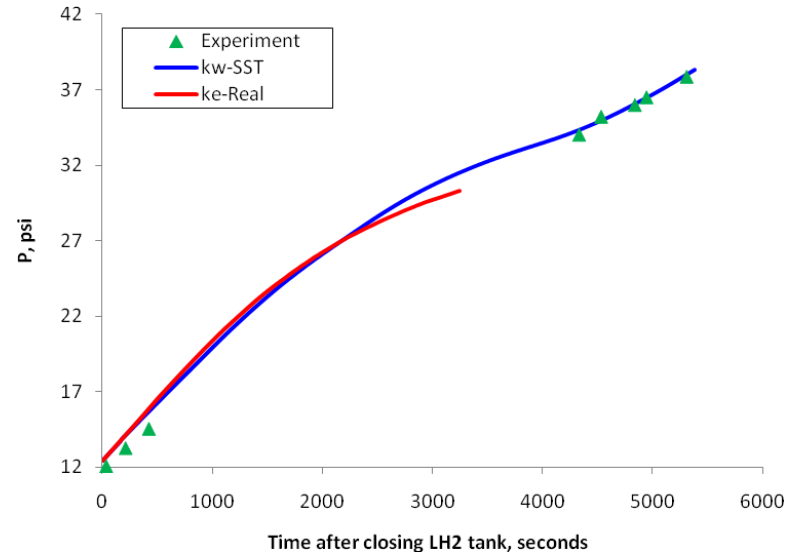

Figure 4. Pressure evolution in the Saturn-IVB tank during closed tank stage (Turbulence model effect: kw-SST versus ke-Real)

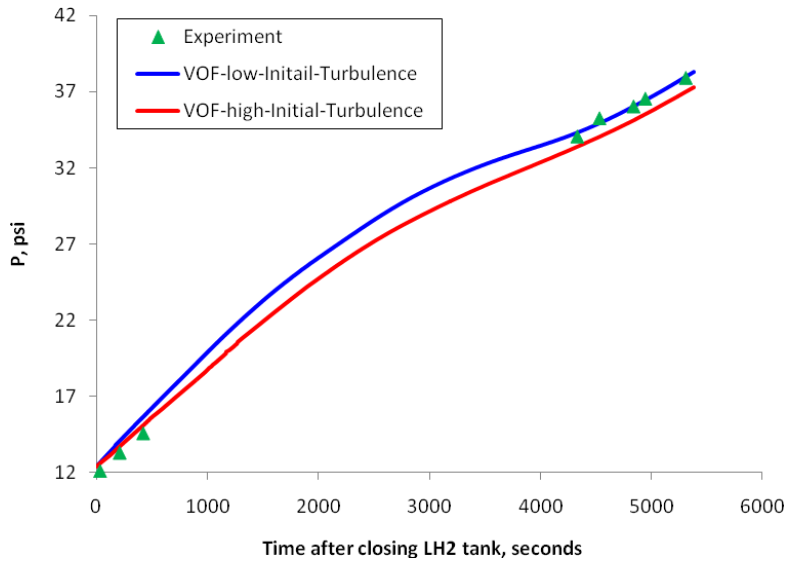

Figure 5. Pressure evolution in the Saturn-IVB tank during closed tank stage (Initial turbulence level effect: low initial turbulence (k = 0.01 m^2/s^2) compared with high initial turbulence (k = 0.1 m^2/s^2)

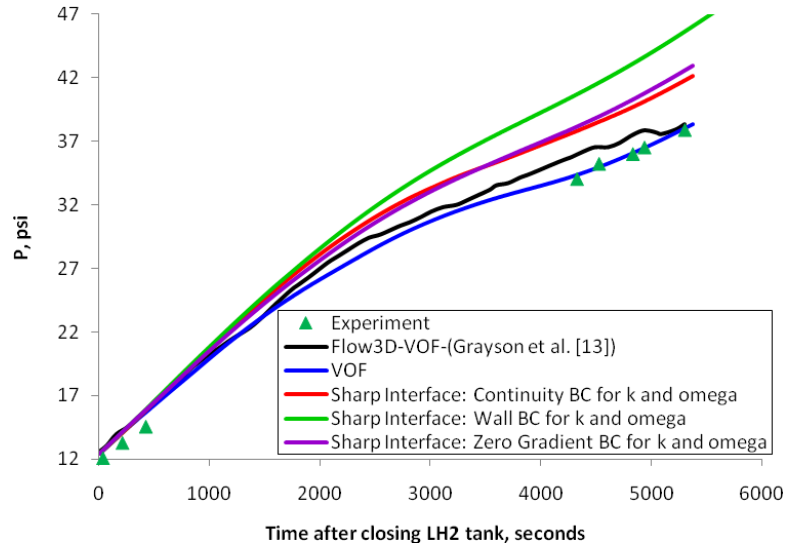

Figure 6. Pressure evolution in the Saturn-IVB tank during closed tank stage (Multiphase model and interfacial turbulence modeling effect)

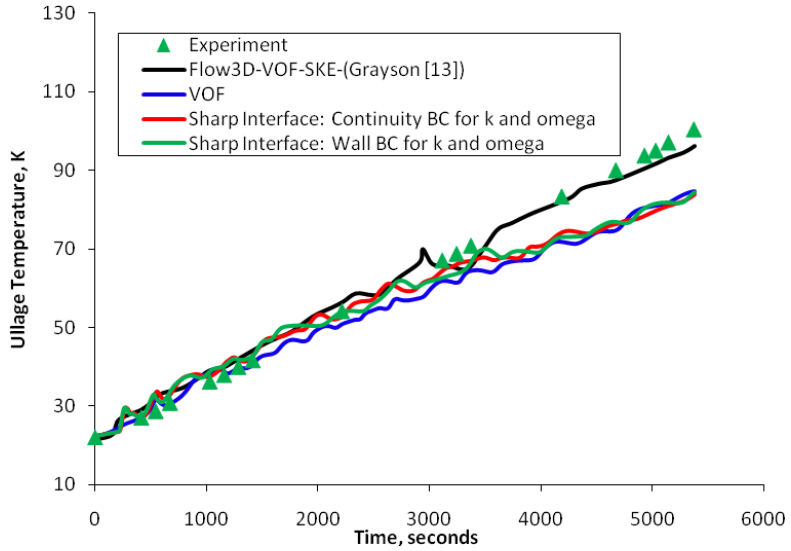

Figure 7. Ullage temperature evolution (temperatue measurement location is at r = 1.68 m, x = 10.21 m, where the bottom of computational domain is located at x = 0 m)

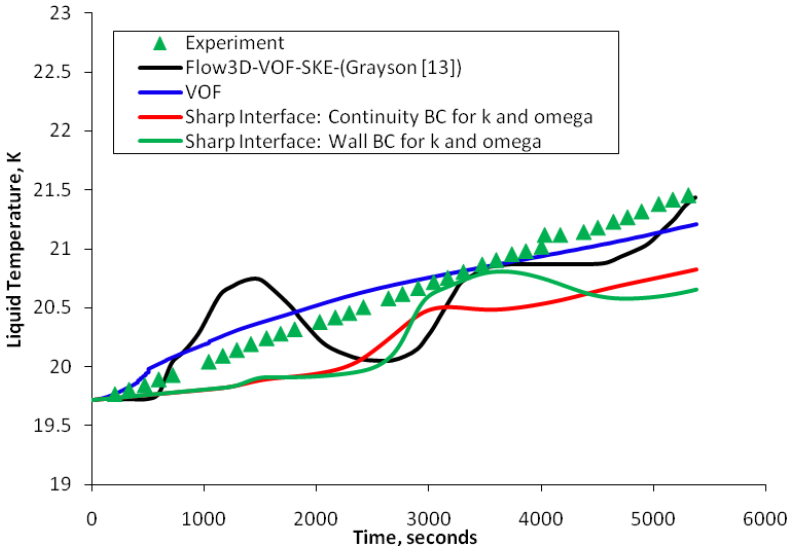

Figure 8. Liquid temperature evolution (temperatue measurement location is at r = 1.68 m, x = 3.03 m, where the bottom of computational domain is located at x = 0 m)

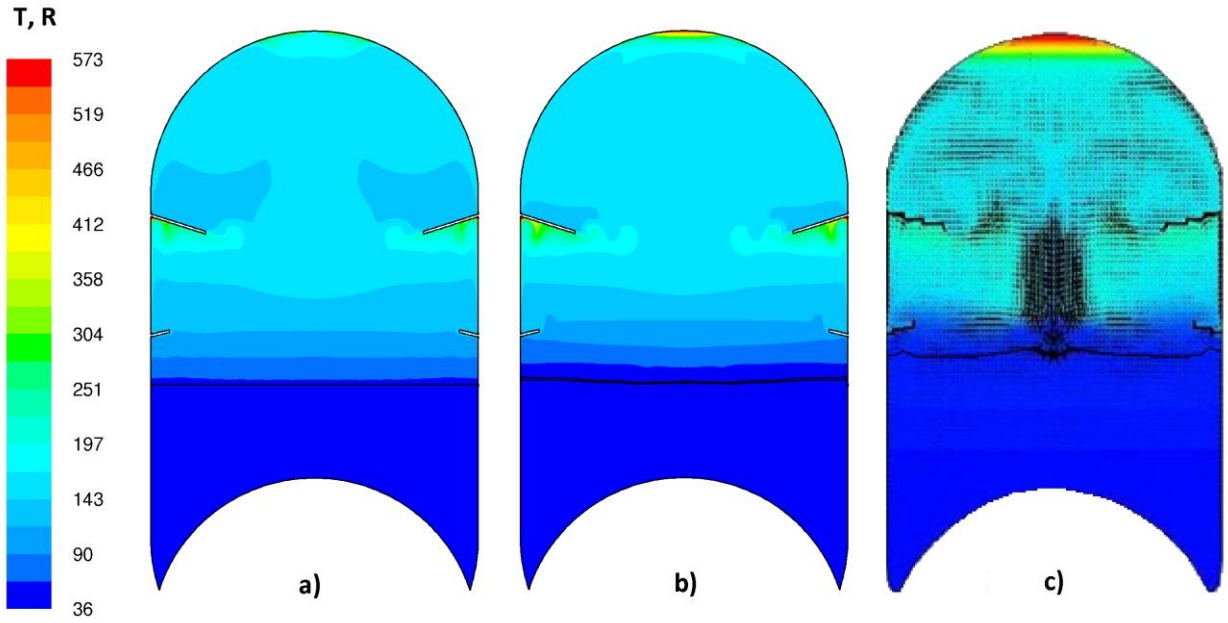

Figure 9. Temperature contours at 5380 seconds of simulation time (a – Sharp Interface model with continuity B.C. for *k* and ω; b – Fluent VOF model; c - Flow3D VOF model of Grayson et al.[13])

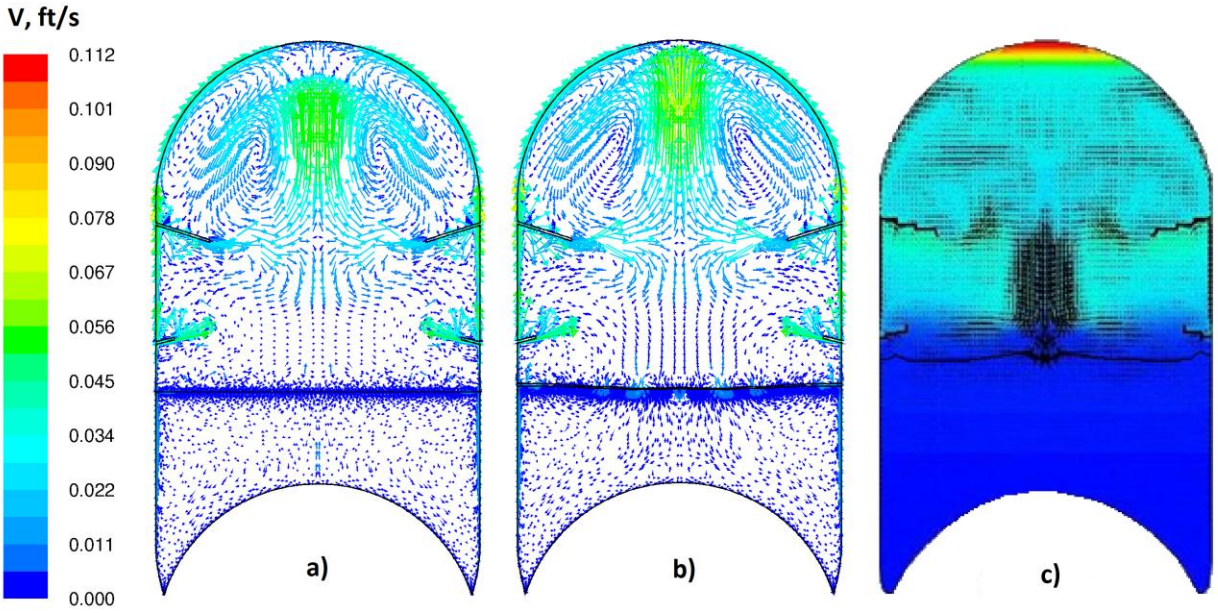

Figure 10. Velocity vectors at 5380 seconds of simulation time time (a – Sharp Interface model with continuity B.C. for *k* and ω; b – Fluent VOF model; c - Flow3D VOF model of Grayson et al.[13])

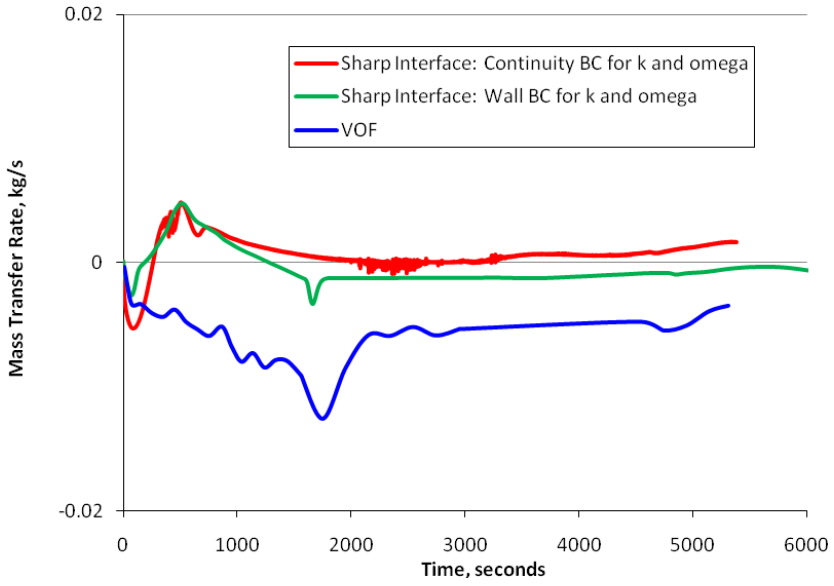

Figure 11. Interfacial mass transfer rate evolution in the Saturn-IVB tank during closed tank stage (Effect of interfacial turbulence modeling with Sharp Interface model compared with the VOF model).

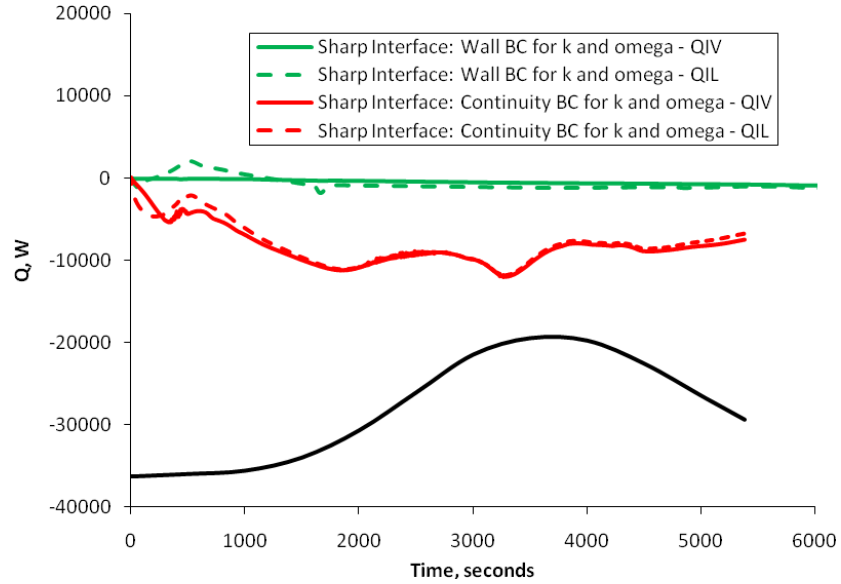

Figure 12. Interfacial heat power evolution in the Saturn-IVB tank during closed tank stage (Effect of interfacial turbulence modeling with Sharp Interface model).

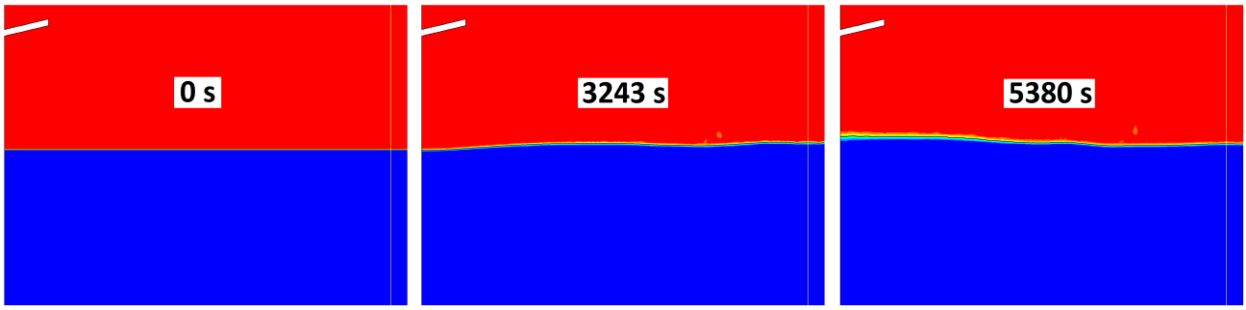

Figure 13. Phase distribution at 0 seconds, 3243 seconds and 5380 seconds of computational time from VOF model with Compressive discretization scheme used for VOF equation (Interfacial area is: 34.21 m^2 at the beginning of simulation when the interface is flat; 34.25 m^2 at 3243 seconds of simulation time; and 34.30 m^2 at the end of simulation).

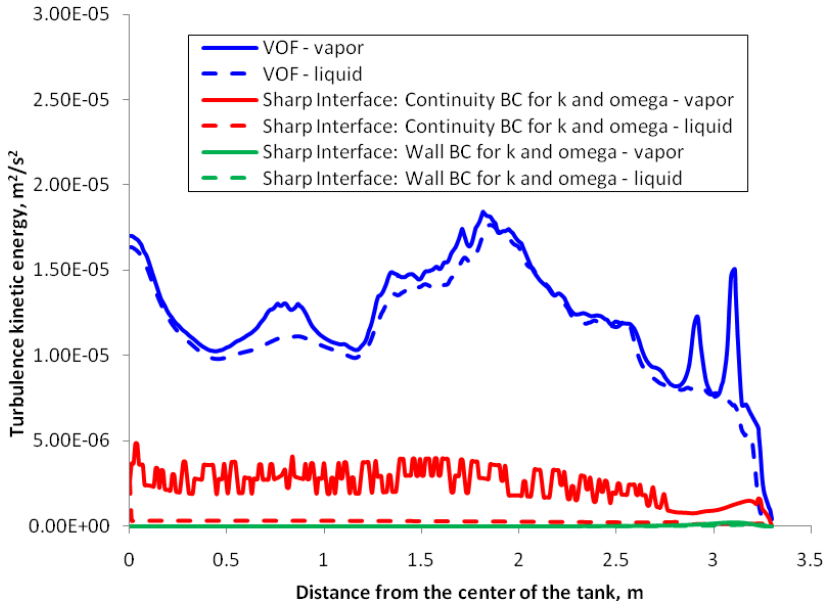

Figure 14. Turbulence kinetic energy at the end of simualtion at 5380 seconds of simulation time. Sharp Interface models with the Wall and Continuty B.C. for k and ω at the interface are compared with the VOF model.

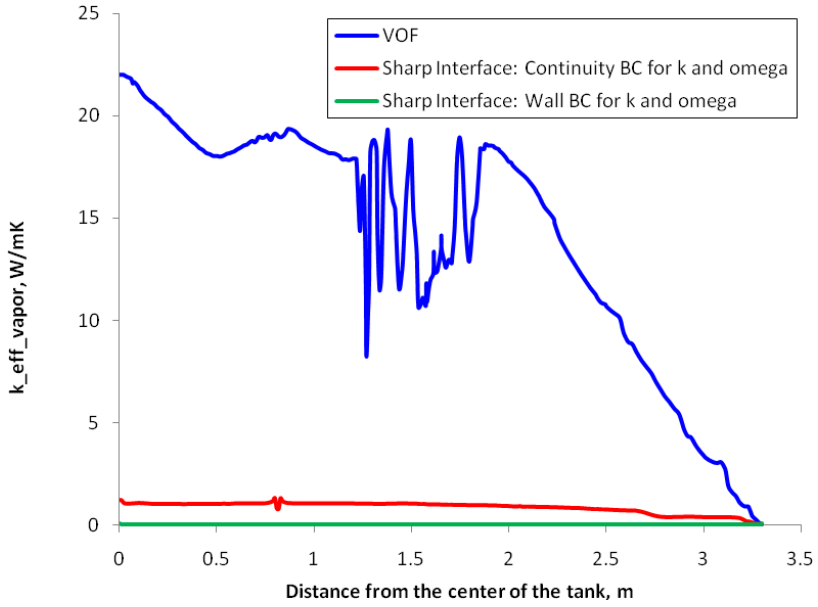

a)

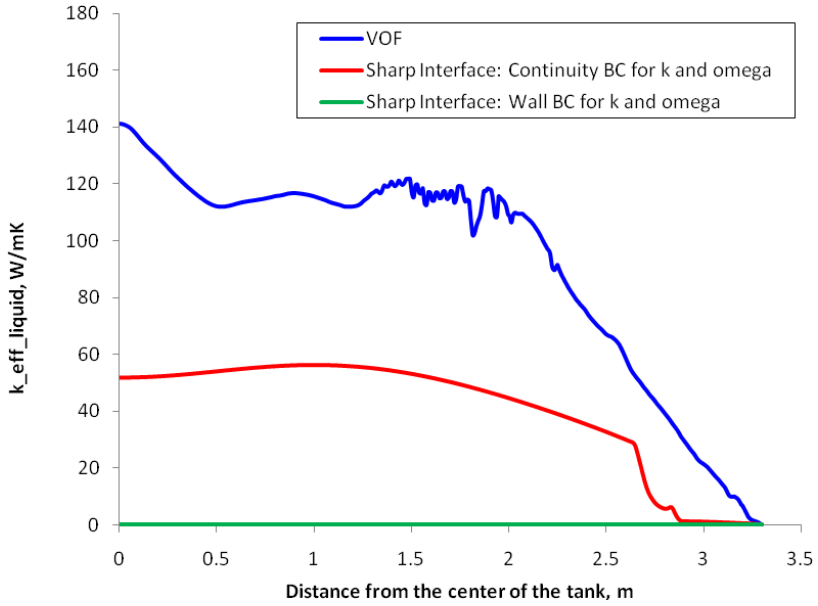

b)

Figure 15. Effective thermal conductivity at the end of simualtion at 5380 seconds of simulation time. Sharp Interface models with the Wall and Continuty B.C. for *k* and ω at the interface are compared with the VOF model. (a – liquid side of the interface; b – vapor side of the interface).